

Anuradha Kalani, Pradip Kumar Kamat, and Neetu Tyagi



# Diabetic Stroke Severity: Epigenetic Remodeling and Neuronal, Glial, and Vascular Dysfunction



*Diabetes* 2015;64:4260–4271 | DOI: 10.2337/db15-0422

**We determined the mechanism of severity during type 1 diabetic (T1D) stroke (ischemia-reperfusion [IR] injury) that affects potential markers associated with epigenetics, neuronal, glial, and vascular components of the brain with regard to nondiabetic stroke. The study used male genetic T1D *Ins2<sup>+/-</sup>* Akita and wild-type (C57BL/6J) mice. The experimental mice groups were 1) sham, 2) IR, 3) sham<sup>Akita</sup>, and 4) IR<sup>Akita</sup>. Mice were subjected to middle cerebral artery occlusion for 40 min, followed by reperfusion for 24 h. Brain tissues were analyzed for inflammation, neuro-glio-vascular impairments, matrix metalloproteinase (MMP)-9 expression, and epigenetic alterations (DNA methyltransferase-3a [DNMT-3a]; DNA methyltransferase-1 [DNMT-1]; 5-methylcytosine [5-mC]; and 5-hydroxymethylcytosine [5-hmC]). Intracarotid fluorescein isothiocyanate-BSA infusion was used to determine pial-venular permeability. IR<sup>Akita</sup> mice showed more infarct volume, edema, inflammation, and vascular MMP-9 expression compared with IR and sham groups. Sham<sup>Akita</sup> mice showed the highest DNMT-1 and DNMT-3a levels compared with the other groups. Reduced tight and adherent junction expressions and severe venular leakage exemplified intense cerebrovascular impairment in IR<sup>Akita</sup> mice compared with the other groups. Interestingly, we found differential regulations (downregulated expression) of epigenetic (5-mC, DNMTs), vascular (endothelial nitric oxide synthase), glial (connexin-43, glial fibrillary acidic protein, CD11b), and neuronal (neuron-specific enolase, neuronal nitric oxide synthase) markers in IR<sup>Akita</sup> compared with the IR group. These findings suggest that IR injury in T1D is more severe because it intensifies differential epigenetic markers and neuro-glio-vascular changes compared with nondiabetic mice.**

Type 1 diabetes (T1D) is a major risk factor for ischemic cerebrovascular disease that increases morbidity and mortality worldwide (1,2). Stroke occurs fivefold more often in patients with T1D and results in intense consequences compared with those in patients without diabetes; however, the mechanisms underlying stroke severity in patients with diabetes are unclear (3). Also, whether stroke is different in people with and without diabetes is unclear. Therefore, understanding these molecular changes and functional relationships with altered regulatory pathways can help explain the conceptual basis behind the severity of stroke in patients with diabetes. In addition, exploring the regulatory pathways and molecular mechanisms may be helpful in the future for designing preventive and therapeutic strategies.

The role of epigenetics was recently broadly characterized and found to be involved in the pathophysiology of stroke. Large clinical trials, such as the Diabetes Control and Complications Trial (DCCT) and Epidemiology of Diabetic Interventions and Complications Trial (EDIC), along with animal studies, have confirmed that hyperglycemia predisposes individuals to develop complications of diabetes, also referred to as the legacy effect (4,5). These reports suggest that hyperglycemia exposure mediates long-lasting epigenetic modifications that intensify global gene expressions by epigenetics modifications. Hence, exploring epigenetic factors underlying diabetic stroke is the need of the hour to better understand the basis of severity in patients with diabetes during stroke.

Epigenetic modifications, for example, DNA methylation, regulate phenotype and gene expression patterns and occur

Department of Physiology and Biophysics, School of Medicine, University of Louisville, Louisville, KY

Corresponding author: Neetu Tyagi, n0tyag01@louisville.edu.

Received 27 March 2015 and accepted 28 August 2015.

This article contains Supplementary Data online at <http://diabetes.diabetesjournals.org/lookup/suppl/doi:10.2337/db15-0422/-/DC1>.

© 2015 by the American Diabetes Association. Readers may use this article as long as the work is properly cited, the use is educational and not for profit, and the work is not altered.

through the aid of enzymatic activity of DNA methyltransferases (DNMTs). Methylation usually occurs at the fifth carbon atom of cytosine residues and forms 5-methylcytosine (5-mC), which may be further oxidized to 5-hydroxymethylcytosine (5-hmC) (6,7). Studying DNMTs and global 5-mCs and 5-hmCs for their biological roles is of great scientific interest that may help in determining gene expression in the diseased and nondiseased state. Whereas 5-mC predicts a compacting chromatin inaccessible to transcription, 5-hmC determines efficient chromatin transcription. However, global 5-mC and 5-hmC levels in diabetic stroke have not been studied.

Specialized endothelial cells line the cerebral vessels and are enwrapped with pericytes and astrocytes that in turn connect to neurons providing nursing and maintenance. A number of different factors, including the extracellular matrix, tight junctions (TJs), pericytes, and astrocyte end-feet, together with adherens junctions, form junctional complexes and play a central role in the control of blood-brain barrier (BBB) integrity (8,9). Disruption in BBB integrity causes BBB permeability, which is manifested by the activation of matrix metalloproteinase-9 (MMP-9) that chops off junction barriers (10). Dysfunction of the BBB advances to stroke-like pathologies by increasing microvascular permeability that in turn affects the neuronal, glial, and vascular system. However, the roles of BBB and neuro-glio-vascular dysfunction in diabetic stroke pathology have not been studied much. The regulatory functions of vascular and neuronal integrity are essentially regulated by nitric oxide (NO) synthase (NOS) enzymes. The NOS enzymes produce NO, which regulates vascular tone, insulin secretion, and neuronal development via different isozymes, for example, endothelial NOS (eNOS) and neuronal NOS (nNOS). NOS regulation has been studied in ischemic injury, but an explanation is needed of its significance in diabetic stroke.

Our goal in the current study was to address two aspects: first, to explore whether ischemia-reperfusion (IR) injury in T1D severely disturbs the neuro-glio-vascular unit by causing intense inflammation, global alteration in epigenetic markers, and high MMP-9 activation, and second, to compare IR injury in T1D with non-T1D to find out the basis of IR injury severity in diabetes.

## RESEARCH DESIGN AND METHODS

### Animals

All animal procedures were conducted at the University of Louisville Health Sciences Center, were in compliance with guidelines established by the National Institutes of Health Guide for the Care and Use of Laboratory Animals, and were approved by the University of Louisville Institutional Animal Care and Use Committee. Male wild-type (WT; C57BL/6J) and Akita (genetic T1D mice, C57BL/6-Ins2<sup>Akita</sup>/J) mice (8–10 weeks old) were obtained from The Jackson Laboratory (Bar Harbor, ME). The experimental mice groups were 1) sham, 2) IR, 3) sham<sup>Akita</sup>, and 4) IR<sup>Akita</sup>. Akita mice with a glucose level >400 mg/dL were used in the study. We assessed inflammatory (tumor necrosis factor- $\alpha$

[TNF- $\alpha$ ], interleukin-6 [IL-6]) and anti-inflammatory (IL-10) cytokines and glial markers (glial fibrillary acidic protein [GFAP]), integrin- $\alpha$  M [CD11b]) using real-time quantitative (q)-PCR. Neuronal (neuronal nuclei [NeuN], neuronal-specific enolase [NSE], nNOS), vascular (zona occluden-1 [ZO-1], claudin-5, eNOS), and epigenetic (DNMT-1 and DNMT-3a) markers were determined using Western blot. MMP-9, vascular (vascular endothelial [VE]-cadherin, occludin), glial (connexin-43 [Cx-43], GFAP), and neuronal (NeuN) markers were quantified using immunohistochemistry (IHC) analysis.

### Animal Surgical Procedure

All mice were allowed free movement in the cage (4–5 mice/cage) and free access to water and food. The mice were maintained at 12/12-h day-night cycle at  $\sim 23^{\circ}\text{C}$  room temperature. Mice were fasted overnight with free access to water just before the day of surgery. At the day of surgery, the mice were transferred to the surgery room, anesthetized with pentobarbital (50 mg/kg body weight), and operated on within 1 h. Anesthetized mice were orally intubated, mechanically ventilated, and the body temperature was maintained at  $37 \pm 1^{\circ}\text{C}$  during surgery.

The common carotid artery was exposed through a midline neck incision and dissected free of the surrounding nerves. Lysine-coated monofilament (2-cm long; 5-0 or 6-0 [11,12]) was inserted into the left external carotid artery, advanced into the internal carotid artery, and wedged into the cerebral arterial circle to obstruct the origin of the middle cerebral artery. After 40 min of surgery, the filament was withdrawn to allow reperfusion for 1 day. The same anesthesia and surgical procedures, except the insertion of filament, were performed in sham groups of mice (13).

Mice were assessed with neurobehavioral tests after IR injury to determine ischemia severity. Neurological deficit scores were graded 0–12 (normal score = 0, maximum score = 12) after the mice performed several behavioral tests, including posture relax test, forelimb placing test, circling, and motor coordination tests. Only mice with a high-grade neurological deficit ( $\geq 9$ ) were used for the study (14,15).

### Microvascular Leakage Assessment

Microvascular permeability was measured as described earlier (10). Mice were anesthetized with pentobarbital sodium (50 mg/kg i.p.). A heating pad was used to maintain body temperature of the mice at  $37 \pm 1^{\circ}\text{C}$ . A 14-mm hole was made in the skull using a high-speed microdrill (Fine Scientific, Foster City, CA). Fluorescein isothiocyanate (FITC)-conjugated BSA (BSA-FITC-albumin, 300  $\mu\text{g}/\text{mL}$ ) was infused through carotid artery cannulation. In vivo imaging with a BX61WI fluorescent microscope (Olympus, Tokyo, Japan) was used to examine the exposed area of the skull. Venules were identified by the topology of the pial circulation and blood flow direction. Selected third-order venular segments were recorded and used as the baseline. After the baseline reading was obtained, images of the venular segments were recorded. The lamp power

and camera gain settings were held constant during the experiments. Data were interpreted with the software provided with the instrument and Image-Pro Plus 6.3 software (Media Cybernetics, Bethesda, MD). Leakage of FITC-BSA was assessed by changes in the ratio of fluorescence intensity in the interstitium to that inside the vessel. The results were averaged and presented.

### Collection of Brain Samples

Brain samples were collected for Western blot, q-PCR, and IHC analysis. The brain tissue samples were harvested from the experimental mice groups, washed with 50 mmol/L PBS (pH 7.4), and stored at  $-80^{\circ}\text{C}$  until use.

### SDS-PAGE and Western Blotting

Equal quantities of brain extracts (40  $\mu\text{g}$ ) were run on 10–15% polyacrylamide gel under reducing condition, and separated proteins were transferred to polyvinylidene fluoride membrane using an electrotransfer apparatus (Bio-Rad, Hercules, CA). After blocking with 5% nonfat dry milk for 1 h, the membranes were probed overnight with a primary antibody (eNOS, nNOS, claudin-5, ZO-1, DNMT-3a, DNMT-1, NSE, NeuN) at  $4^{\circ}\text{C}$ . The next day, the blots were probed with appropriate secondary antibody for 2 h at room temperature and were developed using the ChemiDoc XRS+ Molecular Imager (Bio-Rad). The images were recorded in the chemi-program of a gel documentation system (Bio-Rad). The membranes were stripped and reprobed with monoclonal anti-GAPDH antibody (Millipore, Billerica, MA) as a loading control. Each band density was normalized with a respective GAPDH density using Image Lab densitometry software (Bio-Rad).

### Quantitative Gene Expression Analysis

Total RNA from the brain tissue was isolated using TRIzol reagent (Invitrogen, Grand Island, NY), following the manufacturer's instructions. After the quantity and purity of total RNA was confirmed using NanoDrop 1000 (Thermo Fisher Scientific, Waltham, MA), the RNA was reverse transcribed to cDNA according to the manufacturer's protocol (ImProm-II; Invitrogen). cDNA samples were amplified for the given genes using gene-specific primers (GFAP, CD11b, TNF- $\alpha$ , IL-6, IL-10; sequences given in Supplementary Table 1) using Stratagene Mx3000p (Agilent Technologies, Santa Clara, CA). CT values were determined after baseline and threshold adjustments, and the results were expressed in fold expression. The transcript levels of given genes were normalized with Rn18s.

### IHC Analysis

Frozen brain blocks, prepared with optimal cutting temperature media (Triangle Biomedical Sciences, Durham, NC), were cut into 20- $\mu\text{m}$  sections using a Leica CM cryostat (Leica Microsystems, Buffalo Grove, IL). After removing the mounting matrix and fixing with methanol for 10 min, tissues were blocked with blocking solution (0.1% Triton X-100 TBS, 0.5% BSA, and 10% normal donkey serum) for 1 h at room temperature. The sections were incubated

with primary antibody (MMP-9, occludin, VE-cadherin, NeuN, GFAP, Cx-43) overnight at  $4^{\circ}\text{C}$ . After incubation with the appropriate fluorescence secondary antibodies for 60 min at room temperature, the sections were stained with DAPI (1:10,000) and mounted with antifade mounting media. Images were acquired using a FluoView 1000 laser scanning confocal microscope (Olympus, Allentown, PA), and the data were analyzed with Image-Pro Plus image analysis software.

### Quantification of the 5-mC and 5-hmC Levels

Genomic DNA was isolated (Sigma-Aldrich, St. Louis, MO) from the brain sample, and total 5-mC and 5-hmC levels were determined using ELISA kits (Epigentek, Farmingdale, NY), according to the manufacturer's instructions.

### Fluoro-Jade C Staining

Fluoro-Jade C (FJC) stain (Sigma-Aldrich) was used to determine the presence of neuronal damage. Brain sections were processed according to the method described previously (16). Briefly, paraffin-embedded sections were deparaffinized, rehydrated, and transferred to 0.06% potassium permanganate solution for 10 min. Afterward the sections were incubated in a 0.0001% solution of FJC for 20 min and mounted with DPX. Images were captured, and the data were analyzed with Image-Pro Plus image analysis software.

### Determination of Infarct Volume

Coronal sections (2 mm) were cut using a mouse brain slice matrix (Harvard Apparatus, Holliston, MA). The slices were stained for 20 min at  $37^{\circ}\text{C}$  with 2% 2,3,5-triphenyltetrazolium chloride (Sigma-Aldrich) and postfixed with 4% paraformaldehyde. Infarct area (pale white) of each brain section was determined with Image-Pro Plus image analysis software.

### Cerebral Edema

The cortical parts of the brain ipsilateral area were dried for 3 days in a drying oven at  $100^{\circ}\text{C}$ . The absolute water content was calculated as water content (%) = [(wet weight – dry weight)/wet weight]  $\times$  100.

### Statistical Analysis

All values are expressed as mean  $\pm$  SEM. Statistical comparisons between two groups were performed by the Student *t* test. One-way ANOVA was used for more than two groups. A *P* value of  $<0.05$  was considered to be statistically significant.

## RESULTS

### IR<sup>Akita</sup> Developed Larger Infarct Size, Edema, Inflammation, and Cell Death

IR<sup>Akita</sup> mice showed more infarct size (Fig. 1A and B), cerebral edema (Fig. 1C), proinflammatory cytokines (TNF- $\alpha$  and IL-6), and reduced anti-inflammatory cytokines (IL-10; Fig. 1D) compared with IR and sham<sup>Akita</sup> groups. Cresyl violet staining demonstrated significant degradation of the cellular constituents as indicated by cell swelling (blubbing), decreased cell size (shrinkage), and extensively decreased

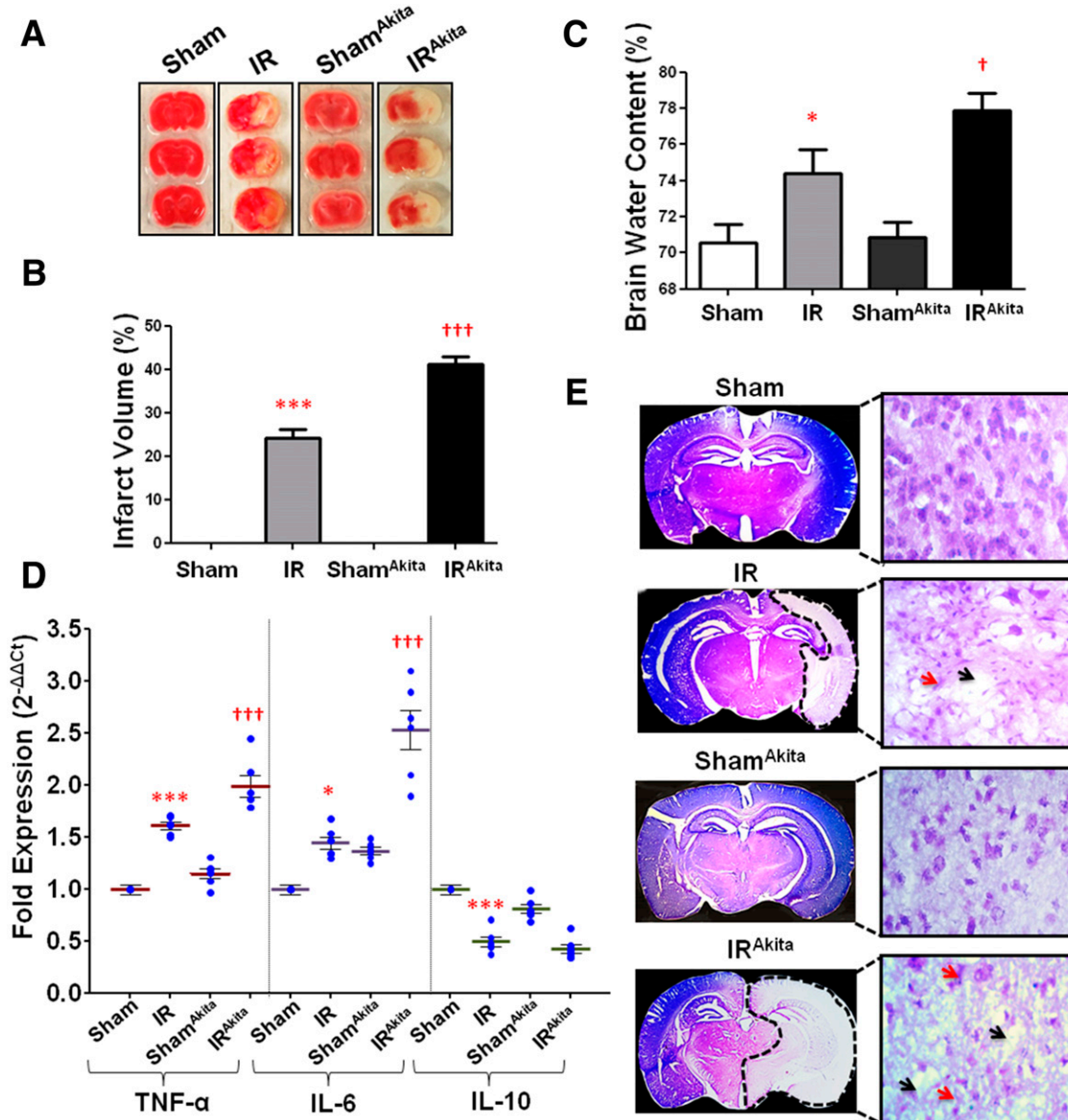


**Figure 1**—Severity of IR injury in the diabetic group. *A*: Mice brain coronal sections stained with 2,3,5-triphenyltetrazolium chloride show infarct volume (white region). *B*: Bar graph shows analysis of infarct volume in different mice groups ( $n = 12$ ). *C*: Bar graph shows brain water content ( $n = 8$ ). *D*: q-PCR analysis shows expression of proinflammatory cytokines TNF- $\alpha$  and IL-6 and anti-inflammatory cytokine IL-10 ( $n = 6$ ). *E*: Representative cresyl violet-stained brains (whole brain coronal sections in the left panel and expanded views in the right panel) show cellular alterations. Cellular changes are represented by red arrows and tissue disintegration is shown by black arrows ( $n = 4$ ). The dotted lines encircle the infarct area of the brain sections. \* $P < 0.05$ , \*\*\* $P < 0.001$  vs. sham; † $P < 0.05$ , ††† $P < 0.001$  vs. IR.

cell number in the IR<sup>Akita</sup> group compared with the sham, IR, and sham<sup>Akita</sup> groups (Fig. 1E). These results indicate severe IR-injury in diabetic mice compared with nondiabetic mice.

**Diabetic Brain With Stroke Exhibited Intense Epigenetic Remodeling**

To address potential markers associated with epigenetics, mice brains were evaluated for levels of DNMTs and global %5-mC and %5-hmC levels. Western blots exemplified the highest protein expression of DNMT-1 and -3a in the sham<sup>Akita</sup> group. The IR group exhibited a significant

increase in DNMT-1 and -3a protein levels compared with the sham group, and the IR<sup>Akita</sup> group showed a considerable decrease in DNMT-1 and -3a compared with the sham<sup>Akita</sup> group (Fig. 2A and B). Furthermore, the IR group showed an increase in global 5-mC levels and a decrease in global 5-hmC levels compared with the sham group, and the IR<sup>Akita</sup> group showed a decrease in global 5-mC and 5-hmC levels compared with the sham<sup>Akita</sup> group (Fig. 2C and D). Hence, DNMTs and 5-mC levels were increased in the IR group and decreased in IR<sup>Akita</sup> group compared with the sham and sham<sup>Akita</sup> groups, respectively. These results represented differential

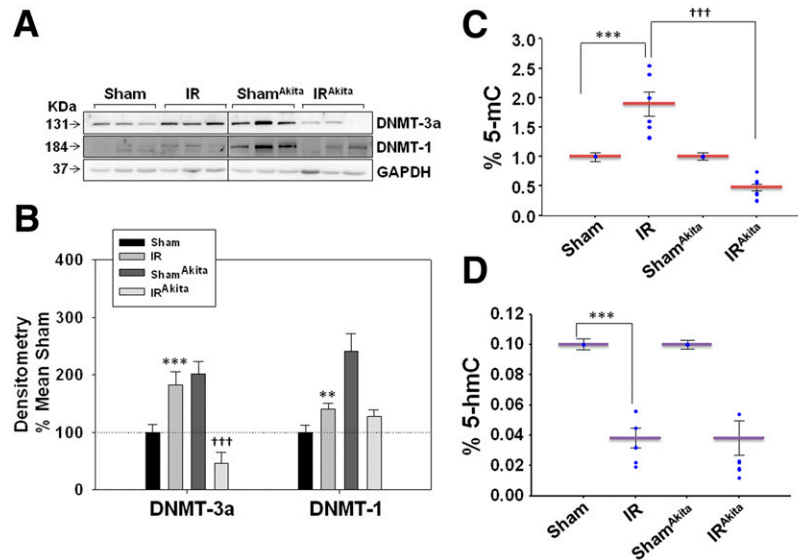


**Figure 2**—Epigenetic remodeling during IR injury in diabetic and nondiabetic mice. *A*: Representative Western blot images show DNMT-3a and DNMT-1 protein expressions in different experimental mice groups. Each lane represents a different mouse sample. The two panels in Western blot represent two gels run at the same time under the same experimental conditions. *B*: Densitometry summary is dictated by the bar graph showing normalized DNMT-3a and DNMT-1 protein expressions with GAPDH ( $n = 5$ ). Charts representing absolute quantification of global %5-mC (*C*) and %5-hmC (*D*) in different experimental mice brains. The data are calculated through standardized subsets of 5-mC and 5-hmC standards, and the test values are described in percentages ( $n = 6$ ). \*\* $P < 0.01$ , \*\*\* $P < 0.001$  vs. sham; ††† $P < 0.001$  vs. IR.

epigenetic remodeling after IR injury in diabetic versus nondiabetic mice.

### IR<sup>Akita</sup> Brains Showed Severe Vascular Injury and BBB Disruption

Intracarotid FITC-BSA infusion exemplified the highest macromolecular pial venular permeability in the IR<sup>Akita</sup> group. The IR and sham<sup>Akita</sup> groups also exhibited considerable high venular permeability compared with the sham group (Fig. 3*A* and *B*). We further evaluated endothelial junction proteins because these actively regulate selective barrier functions across the vessel walls. IHC analysis using endothelial junction proteins (occludin and VE-cadherin) determined drastically reduced expression in the cortical vessels of the IR and IR<sup>Akita</sup> groups compared with their respective sham groups (Fig. 3*C* and *D*). Similarly, Western blot analysis using TJs (ZO-1 and claudin-5) confirmed remarkably decreased expressions in the IR<sup>Akita</sup> group compared with the sham, IR, and sham<sup>Akita</sup> groups (Fig. 3*E* and *F*). Protein expressions of ZO-1 and claudin-5 were also considerably reduced in the IR and sham<sup>Akita</sup> groups compared with the sham group (Fig. 3*E* and *F*). Because the vascular impairment is exacerbated with MMP-9 activation, we further determined vascular MMP-9 expression using IHC analysis. The highest elevation in vascular MMP-9 expression among the different groups was observed in the IR<sup>Akita</sup> group. However, significant enhancement in vascular MMP-9 was also observed in the IR and sham<sup>Akita</sup> groups compared with the sham group (Fig. 3*G* and *H*).

### IR<sup>Akita</sup> Showed Disrupted Glia After Stroke

To address glial markers, we determined transcript levels of GFAP and CD11b using q-PCR analysis. Whereas the IR group showed significantly increased GFAP and CD11b mRNA levels, the IR<sup>Akita</sup> group showed a noticeable decrease in GFAP and CD11b mRNA compared with their respective shams. GFAP and CD11b were also significantly high in the sham<sup>Akita</sup> mice compared with the sham mice (Fig. 4*A*). To address the vascular connection to glia, we evaluated Cx-43, an astral-gap junction marker, through IHC analysis of cerebral vessels. Extremely reduced immunoreactivity of Cx-43 was observed in the cortical vessels of the IR<sup>Akita</sup> mice compared with the sham<sup>Akita</sup> mice. Conversely, increased Cx-43 immunoreactivity was observed in the IR group compared with the sham group (Fig. 4*B* and *C*). Furthermore, IHC analysis confirmed reduced GFAP immunoreactivity in the hippocampus region of IR-injured Akita brains compared with the other brains, and significant amplification in the GFAP immunoreactivity was observed in sham<sup>Akita</sup> and IR brains compared with sham brains (Fig. 4*D* and *E*). These results showed differential regulation of glial activation after IR injury in diabetic versus nondiabetic conditions.

### Neuronal Loss After IR Injury in IR<sup>Akita</sup> Mice

NeuN staining confirmed notable loss of neurons in the hippocampus region after ischemic injury in IR and IR<sup>Akita</sup> brains compared with their respective shams. Diabetic Akita brains also exhibited decreased NeuN expression compared with sham brains (Fig. 4*D* and *E*). Furthermore,

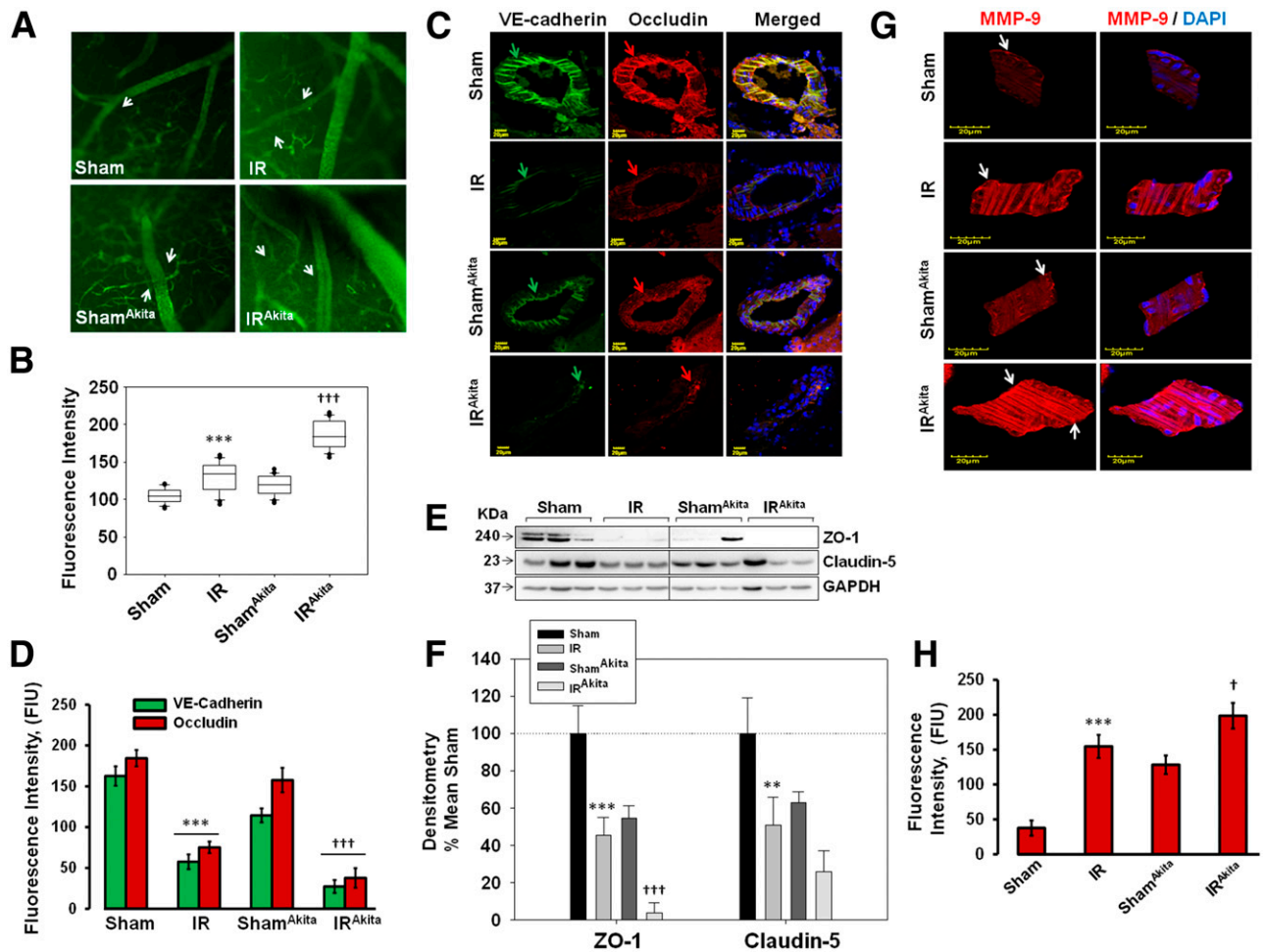


**Figure 3**—Vascular disruption after IR injury in diabetic and nondiabetic groups. *A*: Representative live intravital microscope recorded images show macrovascular leakage through mice brain pial venules (white arrows) using FITC-BSA. *B*: Intensity data were calculated and expressed as fluorescence intensity units (FIU) in the box-and-whisker plot. The horizontal line in the middle of each box indicates the median; the top and bottom borders of the box mark the 75th and 25th percentiles, respectively; the whiskers mark the 90th and 10th percentiles; and the black circles indicate outliers. *C*: Confocal IHC images show VE-cadherin (first lane, green arrow) and occludin (middle lane, red arrow) in mice brain cortical vessels. Merged images are shown in the rightmost lane, along with DAPI-stained cell nuclei (blue). *D*: Analyzed fluorescence intensity of VE-cadherin (green bars) and occludin (red bars) is shown in the bar graph ( $n = 5$ ). *E*: Representative Western blot images show expressions of tight junctions (ZO-1 and claudin-5) with different mice groups. The two panels in Western blot represent two gels run at the same time under the same experimental conditions. *F*: The results of densitometry analysis for ZO-1 and claudin-5 (normalized with GAPDH) are depicted ( $n = 5$ ). *G*: Confocal IHC images show vascular MMP-9 expression (red color, indicated with white arrows) in cerebral vessels of mice brains. *H*: Fluorescent intensity data of MMP-9 are expressed as FIU and represented by the bar graph ( $n = 4$ ).  $^{**}P < 0.01$ ,  $^{***}P < 0.001$  vs. sham;  $^{\dagger}P < 0.05$ ,  $^{\dagger\dagger}P < 0.001$  vs. IR.

Western blot analysis confirmed the lowest expression of NeuN in IR<sup>Akita</sup> brains (Fig. 5A and B). Western blot analysis illustrated reduced expression of NSE, another neuronal-related marker, in the IR<sup>Akita</sup> group compared with the sham<sup>Akita</sup> group. Interestingly, increased expression of NSE was also observed in the IR group compared with the sham group (Fig. 5A and B). We performed FJC staining to address neuronal loss, and the highest degenerating neurons were observed in IR<sup>Akita</sup> brains. FJC staining confirmed neurodegeneration in IR and sham<sup>Akita</sup> brains compared with sham brains (Fig. 5C and D). These results suggested intense neuronal damage during IR injury in diabetes.

**NOS Regulation in IR Injury**

We determined eNOS and nNOS levels that impart main roles in regulating vascular tone and glia and neuronal integrity. Western blot analysis confirmed decreased protein expression of eNOS and nNOS in the IR<sup>Akita</sup> group compared with the sham<sup>Akita</sup> group, while increased eNOS and nNOS expression was observed in the IR group compared with the sham group (Fig. 6A and B). The sham<sup>Akita</sup> group also represented a remarkable increase in nNOS with respect to the sham group (Fig. 6A and B). These data further suggest differential IR injury outcomes in diabetic versus nondiabetic brains.

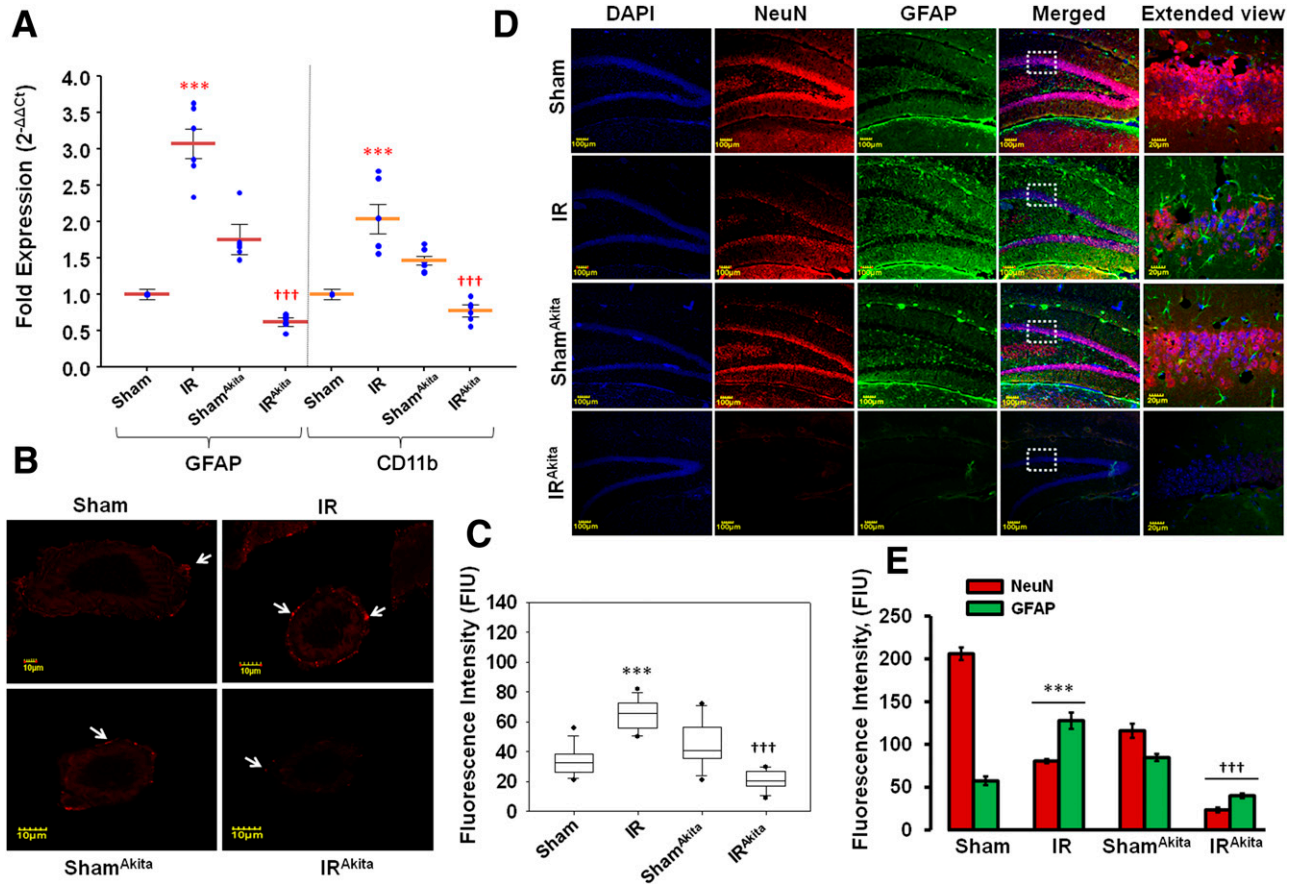


**Figure 4**—Glial expression in diabetic and nondiabetic mice after IR injury. *A*: q-PCR analysis for GFAP (astrocyte specific) and CD11b (microglia specific) in different mice groups ( $n = 6$ ). *B*: Confocal images show Cx-43 (glial gap junction) in cerebral vessels of different mice brains (white arrows). *C*: Fluorescence intensity expressed as fluorescence intensity units (FIU) for Cx-43 was measured in eight cerebral vessels and shown in the box-and-whisker plot. The horizontal line in the middle of each box indicates the median; the top and bottom borders of the box mark the 75th and 25th percentiles, respectively; the whiskers mark the 90th and 10th percentiles; and the black circles indicate outliers. *D*: Confocal images of GFAP (third lane; green) and NeuN (second lane; red) immunoreactivity in the hippocampus region in experimental brains. The left lane shows DAPI-stained cell nuclei (blue), and merged images are shown in fourth lane. All images were captured at original magnification  $\times 10$ . The extended views of the merged images, area in the selected square, are shown at extreme right lane at original magnification  $\times 60$  ( $n = 4$ ). *E*: Bar graph shows fluorescence intensity of NeuN and GFAP. \*\*\* $P < 0.001$  vs. sham; ††† $P < 0.001$  vs. IR.

## DISCUSSION

Our results suggest that IR injury in T1D is severe in infarct volume, intense inflammation, cell death, remodeling of global epigenetic markers, and intense vascular MMP-9 activation. Interestingly, the severity of IR injury in T1D is exacerbated by differential regulations of global epigenetic, vascular, neuronal, and glial functions compared with IR injury in non-T1D.

Although T1D is much less common than type 2 diabetes, the symptoms and injuries are equally abrupt and sometimes more severe. To address the basis of severity in T1D, we performed our studies in the well-established genetic T1D Akita mouse model. Akita mice closely mimic human T1D because they have a genetic defect in the insulin 2 (*Ins2*<sup>+/-</sup>) gene and therefore induce hyperglycemia naturally. Besides that, these mice show higher diabetic traits (blood glucose,  $27.3 \pm 5.3$  mmol/L for males and  $13.6 \pm 3.8$  mmol/L for females), with

decreased reactive immunologically detectable insulin (20.7 to 9.1% in males and 45.9 to 49.6% in females) (17). Akita mice have been used for studying the effects of diabetes on cerebral vasculature (18), sexual dimorphism during diabetes (17,19,20), myelinated fiber loss (21), peripheral neuropathy, and memory performance (22). Akita mice also showed adverse inflammatory and epigenetic remodeling in the heart (23) and impaired vascular density in the brain (18). However, there are no reports of these mice being used to study the effects and mechanisms of ischemic injury. After creating IR injury in Akita hyperglycemic ( $>400$  mg/dL) mice, we found larger cerebral infarcts, more edema, increased cell death, intense inflammation, and reduced anti-inflammation compared with IR-injured nondiabetic mice. We also observed high functional neurological deficits in IR<sup>Akita</sup> mice compared with IR mice. A study of a T1D BioBreeding rat model described the association of diabetic-IR injury with

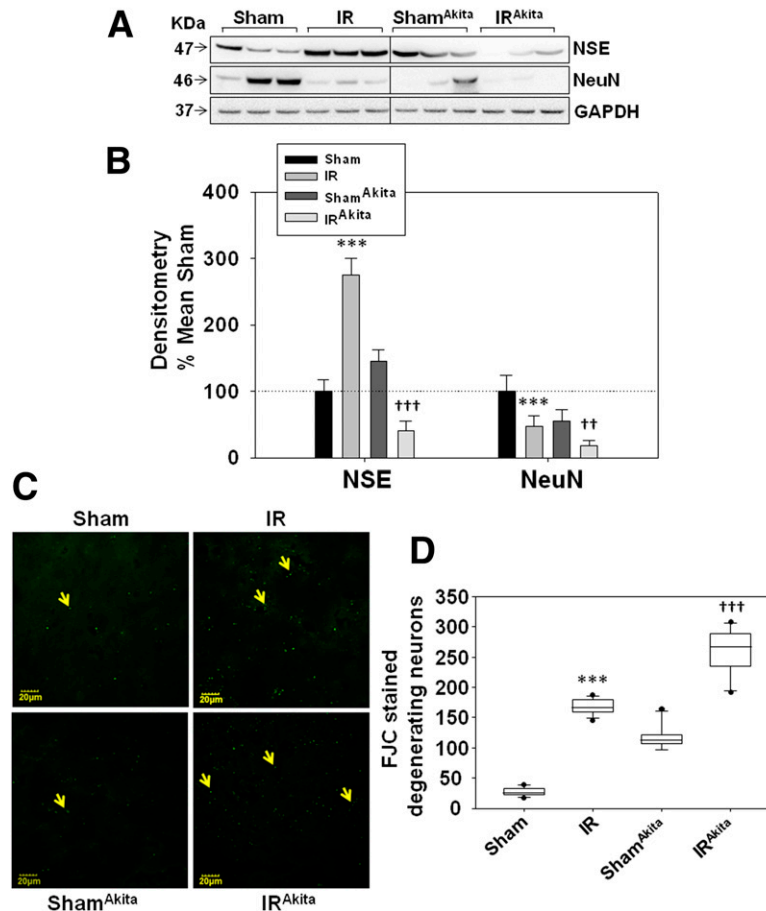


**Figure 5**—Neuronal dysfunction during IR injury in diabetic and nondiabetic mice. Representative Western blot images (A) and bar graphs (B) of the analysis show expression levels of NSE and NeuN in different mice groups ( $n = 6$ ). The two panels in Western blot represent two gels run at the same time under the same experimental conditions. C: Confocal images show FJC-stained degenerating neurons (indicated by yellow arrows) in different mice brains. D: Quantitative analysis for FJC-stained degenerating neurons is shown in the box-and-whisker plot ( $n = 4$ ). The horizontal line in the middle of each box indicates the median; the top and bottom borders of the box mark the 75th and 25th percentiles, respectively; the whiskers mark the 90th and 10th percentiles; and the black circles indicate outliers. \*\*\* $P < 0.001$  vs. sham; †† $P < 0.01$ , ††† $P < 0.001$  vs. IR.

increased infarct size even at tight blood glucose control (24). Similarly, a clinical study that used X-ray computed tomography in 104 patients also confirmed the correlation between hyperglycemia and cerebral infarct size in patients with stroke (25).

The cumulative results of large clinical trials (DCCT, EDIC) and animal studies confirmed the abnormality of the cells under hyperglycemia and invokes phenomenon of altered epigenetics in perpetuating diabetic complications (4,5). Understanding epigenetic modifications may help in exploring novel epigenetic mechanisms that could be targeted for early standpoint or therapeutic aspects against intense ischemic injury during diabetes. We therefore addressed potential epigenetic markers (global %5-mC, %5-hmC, and methylation enzymes). DNMT-1 (maintenance methylation) and DNMT-3a (de novo methylation) were found to be highest in the sham<sup>Akita</sup> group. Our results further showed that DNMT-1, DNMT-3a, and global 5-mC levels were decreased in diabetic brains and

increased in nondiabetic brains after ischemic insult. Stroke in the hyperglycemic state adversely affects potential epigenetic markers that increase the stroke severity in diabetic mice. These results certainly suggest that differential epigenetic alterations can be associated with intense IR injury outcomes in diabetic mice compared with nondiabetic mice. Similar to global %5-mC levels, global %5-hmC levels were also decreased in IR-injured diabetic brains, suggesting sheared and inactive chromatin status that can be associated with intense cellular damage in diabetic brains after ischemia. In agreement with our findings, previous studies have reported an increase in methyltransferases levels in middle cerebral artery occlusion and Akita mice models (23,26,27), and a study of the hippocampus region of 10 patients with Alzheimer's disease found decreased levels of 5-mC and 5-hmC (28). Hence, the decrease of 5-mC and 5-hmC in the study of patients with Alzheimer's disease and in our study suggests that these epigenetic modifications are

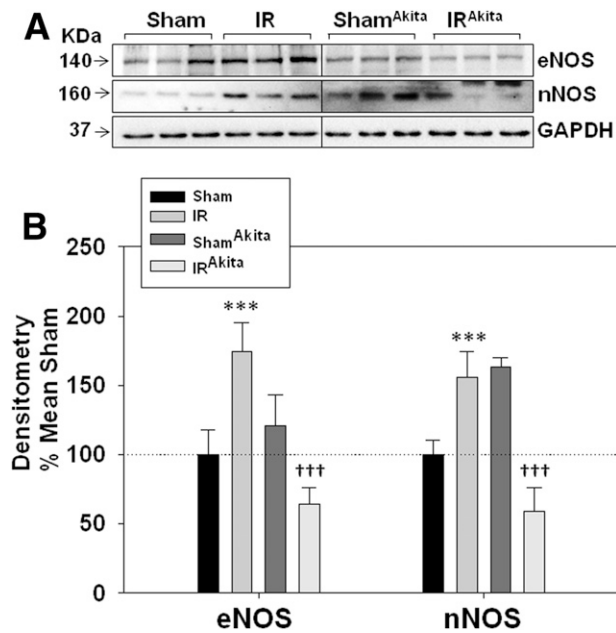


**Figure 6**—Regulation of eNOS and nNOS after IR injury in diabetic and nondiabetic mice. *A*: Representative Western blot images are shown for eNOS and nNOS in different mice groups. Each lane represents a different mouse sample. The two panels in Western blot represent two gels run at the same time under the same experimental conditions. *B*: The densitometry analysis for eNOS and nNOS is shown in the bar graph ( $n = 5$ ). \*\*\* $P < 0.001$  vs. sham; ††† $P < 0.001$  vs. IR.

involved in the pathogenesis of disease. Liyanage et al. (29) reported that there are dynamic changes in DNA methylation that are associated with ischemic injury. Accordingly, it could be suggested that the observed epigenetic changes induce gene expression alterations that ultimately accumulate and develop to disease pathology.

Vascular junctions play a very crucial role in regulating BBB integrity, and their loss is associated with pathogenesis of diseases (10,16). We reported an ~80% decrease in ZO-1 in IR<sup>Akita</sup> versus sham<sup>Akita</sup> mice and an ~57% decrease in ZO-1 in IR versus sham mice. Similarly in claudin-5, there is an ~60% decrease in IR<sup>Akita</sup> versus sham<sup>Akita</sup> mice and an ~40% decrease in IR versus sham. The percentage of the decrease is more in IR<sup>Akita</sup> because the TJs were already disrupted in the diabetic condition and became worse after IR injury. Earlier reports also suggest that the TJs are disrupted in hyperglycemia, corresponding to almost 40% (30).

We further reported functional BBB integrity loss associated with neuro-glia-vascular dysfunction that manifests with intense inflammation and global epigenetic remodeling after IR injury in diabetic mice. Extensive BBB disintegration in IR<sup>Akita</sup> mice increases the chances of blood proinflammatory molecules entering the brain and worsening the IR injury outcomes during diabetes. MMP-9, which is the hallmark for cellular junctions, is activated by inflammation and by creating IR injuries, and we have shown that MMP-9 activation chops off vascular junction proteins and raises BBB permeability (10). In the

current study, we observed more fold change of MMP-9 in IR mice compared with IR<sup>Akita</sup> mice, although the basal level of MMP-9 was high in sham<sup>Akita</sup> compared with WT mice. In agreement, we have reported from our laboratory that the basal expression level of MMP-9 is high in diabetic mice compared with the control (31,32). We observed the highest vascular MMP-9 expression and cerebrovascular permeability in IR-injured diabetic mice, suggesting that persistent hyperglycemia might accelerate brain vasculature and BBB damage. However, controversy remains for subjects with diabetes: on the one hand, sustained BBB integrity was reported (33), whereas on the other hand, increased BBB damage was revealed during diabetes (34). In our study, we found increased BBB permeability in diabetic Akita mice. Previous studies have demonstrated that the ischemic brain in *db/db* mice (type 2 diabetes) and streptozotocin-induced mice and rats (T1D) also exhibits increased cerebrovascular dysfunction (35,36).

A cascade of events is mediated after ischemic brain injury, yielding Ca<sup>2+</sup>-dependent activation of the NOS isoforms nNOS and eNOS (37). The role of NOS isozymes in cerebral ischemia damage was described in the study performed in transgenic mice lacking expression of nNOS or eNOS and in in vitro and in vivo models of cerebral ischemia. The study suggested that nNOS plays key roles in neurodegeneration, whereas eNOS has a prominent role in maintaining cerebral blood flow and preventing neuronal injury (38). By looking at eNOS expression, which serves as a major weapon against different vascular diseases, differential regulation was observed during IR injury in diabetic versus nondiabetic mice, indicating its involvement in enhancement of IR pathology in diabetes.

Intensive vascular injury affects vascular-glia interactions during IR injury in diabetes. Astrocytes, the major glial subtype, establish glial network and communicate through gap junctions. A number of studies reported that astrogliosis, a process of glial activation, increases after an ischemic injury to provide support to the neurons. However, we observed decreased GFAP immunoreactivity against IR injury in diabetic conditions. In agreement with our findings, previous reports suggest that diabetic hyperglycemia inhibited ischemia-induced activation of astrocytes and, therefore, caused damage to astrocytes (39,40), probably due to oxidative damage of DNA (41). An earlier study showed that hyperglycemic Akita mice have decreased gap junction communication in oocytes, as demonstrated by lower expression of Cx-43 (42). Hypoglycemia has been found to induce microglial (CD11b) activation (43), whereas in our study, we found that hyperglycemia induced a decrease of CD11b in IR-injured diabetic mice. The differential regulation of glial, astrocyte, and astrocytic gap junction in IR-injured diabetic versus nondiabetic mice further indicated their probable involvement in IR severity during diabetes. Loss of glial activation in IR<sup>Akita</sup> mice indicated loss of neurons, which was confirmed by FJC and NeuN expressions. FJC and NeuN have previously been used as specific markers for neurons

after ischemic stroke (44) and to confirm the evolving phase of infarction after middle cerebral artery occlusion (45). Furthermore, increased levels of neuronal NSE and nNOS in IR mice, whereas decreased levels in IR<sup>Akita</sup>, also indicated differential regulation of the neuronal microenvironment after an IR insult in diabetic versus nondiabetic mice. The increase of the NSE level in IR mice is in agreement with previous findings (46,47), but the decrease of NSE in IR<sup>Akita</sup> is suggestive of neuronal inability to transcribe NSE due to persistent hyperglycemia. In support, another study showed an increase in the NSE mRNA level in patients with diabetes, but a decrease occurred in subjects with diabetic neuropathy (48).

According to the 2014 National Diabetes Statistics Report, ~29.1 million people, or 9.3% of the U.S. population, have diabetes. In this population, 21.0 million people have been diagnosed with diabetes, and 8.1 million people (~27.8%) with diabetes are undiagnosed. Compared with diagnosed people who receive some treatment, the undiagnosed people face more risk of stroke because they do not receive any treatment. Our study can be helpful in that direction. To show the close resemblance of our mouse model with the population with diabetes receiving some treatment, we treated Akita mice with insulin and observed less stroke severity after creating the IR injury compared with untreated mice (Supplementary Figs. 1 and 2).

Although some reports suggest that DNA methylation levels have been found altered in T1D patients, the information about the effect of antidiabetic therapy on epigenetics is scarce. In concordance with our study, altered epigenetic changes have been observed in the kidney of *db/db* diabetic mice in a tissue-specific manner. The authors further reported aberrant DNA methylation,

changes in histone modifications, and mRNA expression in the diabetic kidney and that these changes were resistant to pioglitazone (49). In another study by Ishikawa et al. (50), there was increase in the DNA methylation of the *Ins1* (insulin 1) promoter in isolated islets from Zucker diabetic fatty rats. However, use of metformin treatment suppressed DNA methylation and upregulated insulin gene expression. Evans-Molina et al. (51) observed 15- and 7-fold increases in expression of *Ins1/2* and *GLUT2* in cultured islets harvested from mice after 6 weeks of oral pioglitazone therapy. These islets also showed increased altered epigenetic modifications, mRNA, and protein levels. Although there are few reports on the effect of antidiabetic therapy on epigenetic markers, literature suggests that with the progression of diabetes, the epigenetic changes are also progressive, although the changes are slowed with the use of antidiabetic therapy. The study data clearly indicate that the stroke effect in the Akita mice was significantly enhanced compared with the stroke effect in the WT mice. The results show strong evidence that epigenetics and neuro-glio-vascular markers are drastically changed in diabetic IR<sup>Akita</sup> mice and contribute to the disease pathology. However, additional studies in this direction are warranted. On the basis of the results obtained, we have proposed a hypothesis that explains the severity in diabetic stroke (Fig. 7).

In summary, our study provides a novel insight in understanding the mechanistic basis of IR injury severity in T1D by comparing with nondiabetic injury. Through the current report we observed differential regulations of epigenetic markers and neuro-glio-vascular components that explain the reasons of IR severity in subjects with diabetes. The involvement of intense inflammation,

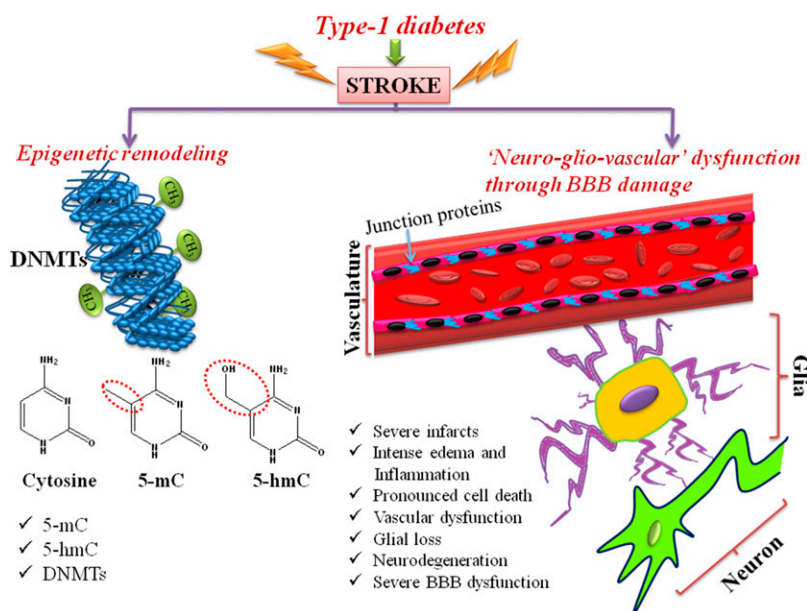


**Figure 7**—The proposed hypothesis for diabetic stroke severity is shown. Stroke during T1D causes altered epigenetic markers and neuro-glio-vascular dysfunction that amplify the severity of the stroke.

potential markers associated with epigenetic alterations, and high vascular MMP-9 activation in diabetes profoundly intensify the injury outcomes. These findings pave the way for further studies that might be helpful in developing better preventive and therapeutic approaches for diabetic stroke.

**Acknowledgments.** The authors are indebted to research volunteer Guoxin Chu, MD, Jilin Province People's Hospital, Changchun, China, for his support and help in the surgical experiments.

**Funding.** This work was supported by a National Institutes of Health grant from the National Heart, Lung, and Blood Institute (HL-107640) to N.T.

**Duality of Interest.** No potential conflicts of interests relevant to this article were reported.

**Author Contributions.** A.K. designed and performed the studies and wrote the manuscript. P.K.K. performed the experiments and participated in the experimental analysis. N.T. obtained the funding, helped in the experiments and with the data analysis, and participated in the writing of the manuscript. All authors approved the final form of the manuscript. N.T. is the guarantor of this work and, as such, had full access to all the data in the study and takes responsibility for the integrity of the data and the accuracy of the data analysis.

## References

- Borch-Johnsen K. The prognosis of insulin-dependent diabetes mellitus. An epidemiological approach. *Dan Med Bull* 1989;36:336–348
- Dorman JS, Laporte RE, Kuller LH, et al. The Pittsburgh insulin-dependent diabetes mellitus (IDDM) morbidity and mortality study. Mortality results. *Diabetes* 1984;33:271–276
- Hägg S, Thorn LM, Putaala J, et al.; FinnDiane Study Group. Incidence of stroke according to presence of diabetic nephropathy and severe diabetic retinopathy in patients with type 1 diabetes. *Diabetes Care* 2013;36:4140–4146
- Miao F, Chen Z, Genuth S, et al.; DCCT/EDIC Research Group. Evaluating the role of epigenetic histone modifications in the metabolic memory of type 1 diabetes. *Diabetes* 2014;63:1748–1762
- Reddy MA, Zhang E, Natarajan R. Epigenetic mechanisms in diabetic complications and metabolic memory. *Diabetologia* 2015;58:443–455
- Chopra P, Papale LA, White AT, et al. Array-based assay detects genome-wide 5-mC and 5-hmC in the brains of humans, non-human primates, and mice. *BMC Genomics* 2014;15:131
- Khare T, Pai S, Koncencius K, et al. 5-hmC in the brain is abundant in synaptic genes and shows differences at the exon-intron boundary. *Nat Struct Mol Biol* 2012;19:1037–1043
- Zlokovic BV. The blood-brain barrier in health and chronic neurodegenerative disorders. *Neuron* 2008;57:178–201
- Nitta T, Hata M, Gotoh S, et al. Size-selective loosening of the blood-brain barrier in claudin-5-deficient mice. *J Cell Biol* 2003;161:653–660
- Kalani A, Kamat PK, Famil'tseva A, et al. Role of microRNA29b in blood-brain barrier dysfunction during hyperhomocysteinemia: an epigenetic mechanism. *J Cereb Blood Flow Metab* 2014;34:1212–1222
- Chiang T, Messing RO, Chou WH. Mouse model of middle cerebral artery occlusion. *J Vis Exp* 2011:2761
- Lee S, Hong Y, Park S, Lee SR, Chang KT, Hong Y. Comparison of surgical methods of transient middle cerebral artery occlusion between rats and mice. *J Vet Med Science* 2014;76:1555–1561
- Tyagi N, Qipshidze N, Munjal C, et al. Tetrahydrocurcumin ameliorates homocysteinylated cytochrome-c mediated autophagy in hyperhomocysteinemia mice after cerebral ischemia. *J Mol Neurosci* 2012;47:128–138
- Belayev L, Alonso OF, Busto R, Zhao W, Ginsberg MD. Middle cerebral artery occlusion in the rat by intraluminal suture. Neurological and pathological evaluation of an improved model. *Stroke* 1996;27:1616–1622; discussion 1623
- Eady TN, Khoutorova L, Anzola DV, et al. Acute treatment with docosa-hexaenoic acid complexed to albumin reduces injury after a permanent focal cerebral ischemia in rats. *PLoS One* 2013;8:e77237
- Kalani A, Kamat PK, Givvimani S, et al. Nutri-epigenetics ameliorates blood-brain barrier damage and neurodegeneration in hyperhomocysteinemia: role of folic acid. *J Mol Neurosci* 2014;52:202–215
- Yoshioka M, Kayo T, Ikeda T, Koizumi A. A novel locus, *Mody4*, distal to *D7Mit189* on chromosome 7 determines early-onset NIDDM in nonobese *C57BL/6* (*Akita*) mutant mice. *Diabetes* 1997;46:887–894
- Givvimani S, Sen U, Tyagi N, Munjal C, Tyagi SC. X-ray imaging of differential vascular density in *MMP-9<sup>-/-</sup>*, *PAR-1<sup>+/-</sup>*, hyperhomocysteinemic (*CBS<sup>-/+</sup>*) and diabetic (*Ins2<sup>-/+</sup>*) mice. *Arch Physiol Biochem* 2011;117:1–7
- Toyoshima M, Asakawa A, Fujimiya M, et al. Dimorphic gene expression patterns of anorexigenic and orexigenic peptides in hypothalamus account male and female hyperphagia in *Akita* type 1 diabetic mice. *Biochem Biophys Res Commun* 2007;352:703–708
- Ueno N, Inui A, Kalra PS, Kalra SP. Leptin transgene expression in the hypothalamus enforces euglycemia in diabetic, insulin-deficient nonobese *Akita* mice and leptin-deficient obese *ob/ob* mice. *Peptides* 2006;27:2332–2342
- Yaguchi M, Nagashima K, Izumi T, Okamoto K. Neuropathological study of *C57BL/6Akita* mouse, type 2 diabetic model: enhanced expression of alphaB-crystallin in oligodendrocytes. *Neuropathology* 2003;23:44–50
- Choeiri C, Hewitt K, Durkin J, Simard CJ, Renaud JM, Messier C. Longitudinal evaluation of memory performance and peripheral neuropathy in the *Ins2C96Y Akita* mice. *Behav Brain Res* 2005;157:31–38
- Chavali V, Tyagi SC, Mishra PK. Differential expression of *dicer*, miRNAs, and inflammatory markers in diabetic *Ins2<sup>+/-</sup>* *Akita* hearts. *Cell Biochem Biophys* 2014;68:25–35
- Toung TK, Hurn PD, Traystman RJ, Sieber FE. Estrogen decreases infarct size after temporary focal ischemia in a genetic model of type 1 diabetes mellitus. *Stroke* 2000;31:2701–2706
- de Falco FA, Sepe Visconti O, Fucci G, Caruso G. Correlation between hyperglycemia and cerebral infarct size in patients with stroke. A clinical and X-ray computed tomography study in 104 patients. *Schweiz Arch Neurol Psychiatr* 1993;144:233–239
- Pandi G, Nakka VP, Dharap A, Roopra A, Vemuganti R. MicroRNA miR-29c down-regulation leading to de-repression of its target DNA methyltransferase 3a promotes ischemic brain damage. *PLoS One* 2013;8:e58039
- Endres M, Fan G, Meisel A, Dirnagl U, Jaenisch R. Effects of cerebral ischemia in mice lacking DNA methyltransferase 1 in post-mitotic neurons. *Neuroreport* 2001;12:3763–3766
- Chouliaras L, Mastroeni D, Delvaux E, et al. Consistent decrease in global DNA methylation and hydroxymethylation in the hippocampus of Alzheimer's disease patients. *Neurobiol Aging* 2013;34:2091–2099
- Liyanage VR, Jarmasz JS, Murugesan N, Del Bigio MR, Rastegar M, Davie JR. DNA modifications: function and applications in normal and disease states. *Biology (Basel)* 2014;3:670–723
- Shao B, Bayraktutan U. Hyperglycaemia promotes cerebral barrier dysfunction through activation of protein kinase C- $\beta$ . *Diabetes Obes Metab* 2013;15:993–999
- Mishra PK, Chavali V, Metreveli N, Tyagi SC. Ablation of MMP9 induces survival and differentiation of cardiac stem cells into cardiomyocytes in the heart of diabetics: a role of extracellular matrix. *Can J Physiol Pharmacol* 2012;90:353–360
- Chaturvedi P, Kalani A, Medina I, Famil'tseva A, Tyagi SC. Cardiosome mediated regulation of MMP9 in diabetic heart: role of mir29b and mir455 in exercise. *J Cell Mol Med* 2015;19:2153–2161
- Dai J, Vrensen GF, Schlingemann RO. Blood-brain barrier integrity is unaltered in human brain cortex with diabetes mellitus. *Brain Res* 2002;954:311–316
- Starr JM, Wardlaw J, Ferguson K, MacLulich A, Deary IJ, Marshall I. Increased blood-brain barrier permeability in type II diabetes demonstrated by gadolinium magnetic resonance imaging. *J Neurol Neurosurg Psychiatry* 2003;74:70–76

35. Chen J, Cui X, Zacharek A, Cui Y, Roberts C, Chopp M. White matter damage and the effect of matrix metalloproteinases in type 2 diabetic mice after stroke. *Stroke* 2011;42:445–452
36. Cui X, Chopp M, Zacharek A, Ye X, Roberts C, Chen J. Angiotensin/Tie2 pathway mediates type 2 diabetes induced vascular damage after cerebral stroke. *Neurobiol Dis* 2011;43:285–292
37. Love S. Oxidative stress in brain ischemia. *Brain Pathol* 1999;9:119–131
38. Samdani AF, Dawson TM, Dawson VL. Nitric oxide synthase in models of focal ischemia. *Stroke* 1997;28:1283–1288
39. Jing L, Mai L, Zhang JZ, et al. Diabetes inhibits cerebral ischemia-induced astrocyte activation - an observation in the cingulate cortex. *Int J Biol Sci* 2013;9:980–988
40. Muranyi M, Ding C, He Q, Lin Y, Li PA. Streptozotocin-induced diabetes causes astrocyte death after ischemia and reperfusion injury. *Diabetes* 2006;55:349–355
41. Jing L, He Q, Zhang JZ, Li PA. Temporal profile of astrocytes and changes of oligodendrocyte-based myelin following middle cerebral artery occlusion in diabetic and non-diabetic rats. *Int J Biol Sci* 2013;9:190–199
42. Chang AS, Dale AN, Moley KH. Maternal diabetes adversely affects pre-ovulatory oocyte maturation, development, and granulosa cell apoptosis. *Endocrinology* 2005;146:2445–2453
43. Won SJ, Kim JH, Yoo BH, et al. Prevention of hypoglycemia-induced neuronal death by minocycline. *J Neuroinflammation* 2012;9:225
44. Liu F, Schafer DP, McCullough LD. TTC, fluoro-Jade B and NeuN staining confirm evolving phases of infarction induced by middle cerebral artery occlusion. *J Neurosci Methods* 2009;179:1–8
45. Huttner HB, Bergmann O, Salehpour M, et al. The age and genomic integrity of neurons after cortical stroke in humans. *Nat Neurosci* 2014;17:801–803
46. Bharosay A, Bharosay VV, Varma M, Saxena K, Sodani A, Saxena R. Correlation of brain biomarker neuron specific enolase (NSE) with degree of disability and neurological worsening in cerebrovascular stroke. *Indian J Clin Biochem* 2012;27:186–190
47. Kim BJ, Kim YJ, Ahn SH, et al. The second elevation of neuron-specific enolase peak after ischemic stroke is associated with hemorrhagic transformation. *J Stroke Cerebrovasc Dis* 2014;23:2437–2443
48. Sandhu HS, Butt AN, Powrie J, Swaminathan R. Measurement of circulating neuron-specific enolase mRNA in diabetes mellitus. *Ann N Y Acad Sci* 2008;1137:258–263
49. Marumo T, Yagi S, Kawarazaki W, et al. Diabetes induces aberrant DNA methylation in the proximal tubules of the kidney. *J Am Soc Nephrol* 2015;26:2388–2397
50. Ishikawa K, Tsunekawa S, Ikeniwa M, et al. Long-term pancreatic beta cell exposure to high levels of glucose but not palmitate induces DNA methylation within the insulin gene promoter and represses transcriptional activity. *PLoS One* 2015;10:e0115350
51. Evans-Molina C, Robbins RD, Kono T, et al. Peroxisome proliferator-activated receptor gamma activation restores islet function in diabetic mice through reduction of endoplasmic reticulum stress and maintenance of euchromatin structure. *Mol Cell Biol* 2009;29:2053–2067